

Field-Free Magnetization Switching Driven by Spin–Orbit Torque in $L1_0$ -FeCrPt Single Layer

Haochang Lyu, Yunchi Zhao,* Jie Qi, He Huang, Jingyan Zhang, Guang Yang, Yaqin Guo, Shipeng Shen, Weidu Qin, Young Sun, Jianxin Shen, Pengwei Dou, Bokai Shao, Yi Zhang, Kui Jin, Youwen Long, Hongxiang Wei, Baogen Shen, and Shouguo Wang*

Electrical switching of magnetization through spin–orbit torque (SOT) induced by a composition gradient in single-layer $L1_0$ -FePt has garnered considerable research interest owing to its inherent superior perpendicular magnetic anisotropy (PMA) that provides ultrahigh capacity to magnetic storage and memory devices. However, a large in-plane external magnetic field is typically required to assist SOT-driven switching, which is still a limitation for the practical application of $L1_0$ -FePt. This study reports realizable field-free magnetization switching by SOT via Cr doping to form a single-layer magnetic structure with an in-plane magnetization component oriented toward $L1_0$ -FeCrPt [110] direction that strongly depends on the magnetocrystalline anisotropy. The Cr doping yields a considerable in-plane exchange-coupling effective field that is conducive toward disintegrating the rotational switching symmetry and facilitates field-free switching in single-layer films with PMA. Furthermore, this in-plane effective field exhibits a nonmonotonic evolution with respect to the Cr-doping concentration, which is validated using first-principles calculation with a frustration-based model of magnetic exchange interactions. Thus, this study delivers an attractive method to facilitate the field-free electrical manipulations of magnetization in single-layer ferromagnets to motivate innovative designs for advanced spintronics devices.

1. Introduction

Spin–orbit torque (SOT) has emerged as a proficient method for electrically manipulating perpendicular magnetization, and it is a promising method for creating ultrafast and reliable advanced-generation spintronic devices.^[1–6] Compared to conventional spin-transfer torque in spin-valves and magnetic tunnel junctions, the SOT requires a significantly lower writing current in modern magnetic-memory technology, thereby improving the energy efficiency and scalability in SOT-based magnetic random-access memory.^[7–9] Prior research reported that such SOT-induced magnetization switching primarily exists in heavy metal/ferromagnet (HM/FM) heterostructures^[1–4,10,11] with strong spin–orbit coupling or single-layer films with bulk noncentrosymmetry such as CuMnAs,^[12] Mn₂Au,^[13] (Ge, Mn)Te,^[14] and (Ga, Mn)As.^[15,16] In addition, the integration of SOT-based devices has been facilitated to induce field-free

H. Lyu, J. Qi, H. Huang, J. Zhang, J. Shen, P. Dou, B. Shao, Y. Zhang, S. Wang

Beijing Advanced Innovation Center for Materials Genome Engineering
School of Materials Science and Engineering
University of Science and Technology Beijing
Beijing 100083, China
E-mail: sgwang@ustb.edu.cn


H. Lyu, Y. Zhao, K. Jin, Y. Long, H. Wei, B. Shen
Beijing National Laboratory for Condensed Matter Physics
Institute of Physics
Chinese Academy of Sciences
Beijing 100190, China
E-mail: yczhao@iphy.ac.cn

G. Yang
School of Integrated Circuit Science and Engineering
Beihang University
Beijing 100191, China

Y. Guo, S. Shen, W. Qin
Institute of Advanced Materials
Beijing Normal University
Beijing 100875, China

Y. Sun
Center of Quantum Materials and Devices
Chongqing University
Chongqing 401331, China

K. Jin, Y. Long
Songshan Lake Materials Laboratory
Dongguan, Guangdong 523808, China

 The ORCID identification number(s) for the author(s) of this article can be found under <https://doi.org/10.1002/adfm.202200660>.

DOI: 10.1002/adfm.202200660

magnetization switching by SOT through several ingenious designs such as the introduction of in-plane exchange bias fields,^[17–19] interlayer exchange coupling,^[20] artificial in-plane symmetry disintegration in structure (lateral composition gradient,^[21] wedged structure,^[22] and geometric engineering^[23]), ferroelectric control,^[24] spin-current manipulations,^[25–27] and crystal-related asymmetry.^[28]

Generally, the origin of SOT in multilayers is considered to arise from the bulk spin Hall effect (SHE) in the heavy metal layer and the Rashba–Edelstein effect (REE) in heterostructure interfaces.^[29] However, traditional SOT in heterostructures characterized by interfacial nature typically requires a very thin FM layer to perform a considerable current-induced switching, which consequently hinders thermal stability and nonvolatility for applications, and the sophisticated design complicates the device structure. Therefore, magnetization manipulation by bulk-nature SOT in a single layer with simple structure offers a promising alternative.

In context, $L1_0$ -ordered FePt possesses considerable application potentials in advanced magnetic materials such as ultra-high-density recording media and high-performance permanent magnets owing to its extremely large perpendicular magnetic anisotropy (PMA) and hard magnetic performance. Moreover, it exhibits excellent thermal stability and compatibility with novel spintronic devices such as magnetic tunneling junctions.^[30–32] Although several strategies have been attempted, the magnetization switching of $L1_0$ -FePt possess insurmountable challenges.^[33–35] Recently, a large bulk-spin torque arising from compositional inversion asymmetry has been observed in a single layer of $L1_0$ -FePt,^[36–38] which can be directly exerted on the magnetic moments for SOT switching. Similar SOT mechanisms have been discussed based on the composition gradient in single-layer GdFeCo^[39] and CoTb^[40,41] films. In single-layer configurations reported to date, the requirement of an external magnetic field for disintegrating the switching symmetry still poses a technological challenge. Although recent studies have demonstrated the realization of field-free SOT switching in a single CoTb layer^[41] owing to the involvement of the gradient-driven Dzyaloshinskii–Moriya interaction (DMI) field as well as the controllable field-free switching in CoPt.^[42] based on the pinned Co layer combined with the in-plane magnetic anisotropy, the corresponding scenario for field-free switching in hard magnetic $L1_0$ -FePt single layer with superior thermal stability has not been implemented to date.

In this study, a deterministic field-free SOT switching was obtained in single $L1_0$ -FePt layers with diluted Cr doping. In this principle, we determined that the addition of Cr induces an in-plane magnetization component oriented toward $L1_0$ -FeCrPt [110] direction along with an enormous in-plane effective field that can equally serve as an external magnetic field to disintegrate the switching symmetry. Moreover, the current results indicated that the in-plane effective field exhibited a nonmonotonic evolution as a function of Cr concentrations. Based on first-principles calculation, a frustration-based model of magnetic exchange interaction was proposed to explain the nonmonotonic variation of the SOT-related effective field. This discovery establishes a new paradigm for achieving SOT switching without any assistance from magnetic fields in single FM alloys, which enables the device integration with advantages

such as simple structure, stable information retention, and ultrahigh thermal stability.

2. Results and Discussion

2.1. Structure and Composition Characterization

FePt alloy with a chemically ordered $L1_0$ structure comprises alternate stacking of Fe and Pt atoms along the c -axis of the face-centered tetragonal (FCT) structure, as depicted in **Figure 1a**. According to a prior study,^[43] the $L1_0$ -ordered structure can be maintained via Cr doping along with canted spins of Fe and Cr (illustrated in Figure 1a). In addition, the epitaxial growth of films can be monitored using in situ reflection high-energy electron diffraction (RHEED). The bright and sharp streaky RHEED patterns displayed in Figure 1b indicate an epitaxial relationship of both $L1_0$ -FePt and $L1_0$ -FeCrPt layers on the MgO substrate. The X-ray diffraction (XRD) spectra illustrated in Figure 1c for 5-nm-thick FePt (blue line) and 5% Cr doped FePt (red line) films exhibit the intense (001) peaks that indicate the formation of a highly ordered FCT structure. Accordingly, the chemical ordering degree S was evaluated with an integrated intensity of (001) and (002) diffraction peaks (refer to Supporting Information S1). After 5% Cr doping, the value of S increased from 0.72 to 0.91, implying an enhanced $L1_0$ ordering. In addition, cross-sectional scanning transmission electron microscopy (STEM) and energy dispersive X-ray spectroscopy (EDS) were performed. The high-resolution high-angle annular dark field (HAADF) image in Figure 1d further demonstrated the high quality of epitaxial $L1_0$ -Fe₄₅Cr₅Pt₅₀ films with single-crystalline structure. More specifically, an enlarged view of the selected region in the inset of Figure 1d depicts a well-defined atomically layered structure, where the brighter atoms indicate Pt and the darker ones represent Fe/Cr atoms. As obtained from EDS mappings, the elemental distributions of Pt, Fe, and Cr are portrayed in Figure 1e–g, which verify an evident Cr doping in the $L1_0$ -ordered lattice of FePt.

2.2. Field-Free SOT Switching Induced by Cr Doping

With the use of conventional lithography and ion milling, the films were fabricated into Hall bar devices with a width of 10 μm to perform transport measurements. Thereafter, current-induced magnetization switching (CIMS) was performed by applying pulsed current (refer to Experimental Section) injected along the x -axis, as illustrated in **Figure 2a**. For archetypical $L1_0$ -FePt structures, the reversible CIMS in 5-nm-thick films can be obtained with the presence of an external magnetic field of ± 1000 Oe (refer to Supporting Information S3) that is consistent with previous studies.^[36–38] Based on an application perspective, a sizable field-free SOT switching of perpendicular magnetization is highly desired to achieve a flexible design of future spintronic devices. In this study, Cr doping was attempted to resolve this limitation. For the $L1_0$ -Fe₄₅Cr₅Pt₅₀ single layer, the anomalous Hall effect (AHE) loop presented in Figure 2b confirmed a maintained PMA. Moreover, the field dependence on CIMS in the 5-nm-thick Fe₄₅Cr₅Pt₅₀ single layer was systematically investigated. The current switching

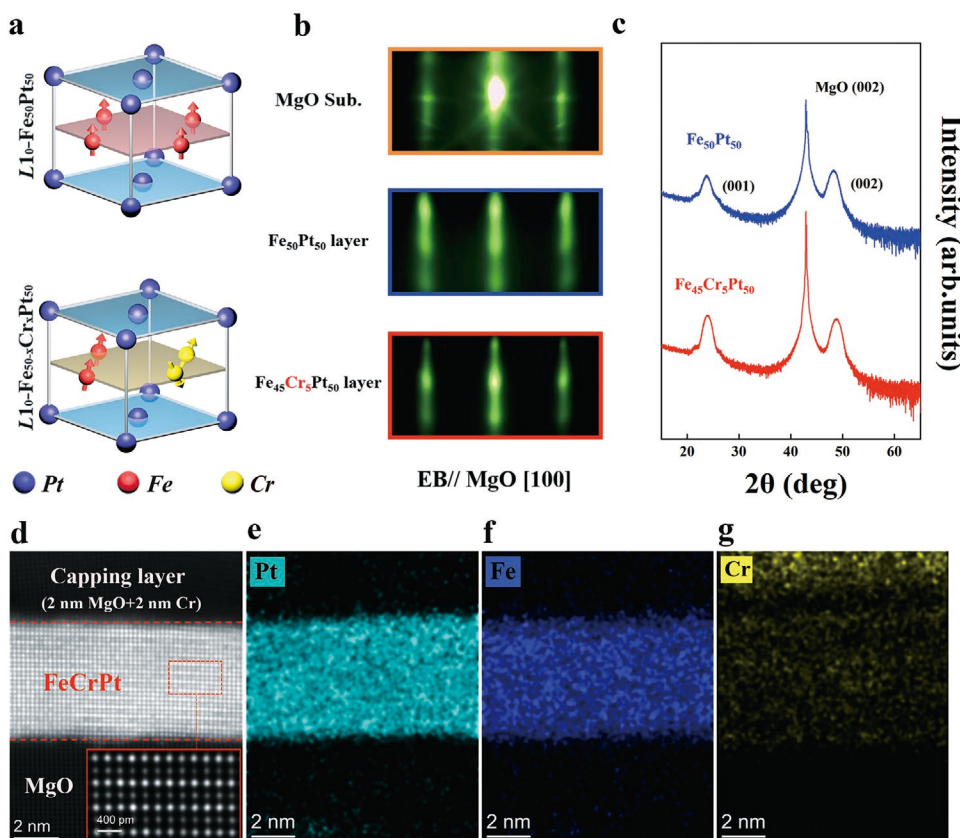


Figure 1. Structure and composition characterization. a) Schematic structure of $L1_0$ -FePt with perpendicular and canted magnetization. b) RHEED patterns for MgO substrate, $L1_0$ -Fe₅₀Pt₅₀ and $L1_0$ -Fe₄₅Cr₅Pt₅₀ layers, respectively, with the e^- -beam along MgO [100] direction. c) XRD spectra of 5-nm-thick Fe₅₀Pt₅₀ and Fe₄₅Cr₅Pt₅₀ films. d) High-resolution HAADF image of Fe₄₅Cr₅Pt₅₀ sample, and enlarged image selected from rectangular region (red dashed line). e–g) EDS mappings of Pt L_{α} , Fe K_{α} , and Cr K_{α} edges corresponding to the region in (d).

loops under varying H_x are exemplified in Figure 2c, where I_p ranging from -22 to $+22$ mA was swept under a static H_x ranging from -2000 to $+2000$ Oe. As expected in the SOT framework, the switching loops suggested opposite switching polarities under large external magnetic fields ($H_x = \pm 2000$ Oe). Overall, the most significant feature is the remarkable SOT-induced magnetization switching in the absence of an external field. This field-free switching loop exhibits the same polarity as the cases with a positive H_x . In addition, almost no switching loop was observed at $H_x = -1000$ Oe, which implies the existence of a large effective intrinsic field participating in the SOT switching process. The critical switching current density J_c is plotted as a function of H_x in Figure 2d. As described in prior research related to SOT switching, J_c is proportional to H_x . In particular, the values of H_x and J_c corresponding to the intersection of their linear fits are defined as H_{x0} and J_{c0} , and estimated as -1000 Oe and 2.7×10^7 A cm^{-2} , respectively. The fitting lines on the right- (red line) and left-hand side (blue line) of $H_x = -1000$ Oe exhibit an intriguing asymmetric behavior. On the contrary, the repeatability of this field-free SOT switching was further investigated by applying successive positive and negative current pulses injected into the device. The successive SOT switching at zero field with a 1 ms duration of current pulses and an interval of 10 s is presented as Figure 2e. The high- and low-resistance states can be cyclically toggled under a

series of current pulses, which signifies a highly stable current-induced magnetization switching performance in the absence of an external magnetic field.

As portrayed in Figure 3a, the angular-dependent transport measurements were conducted by varying the azimuth angles (θ_1) to the [110] direction to obtain the magnitude and direction of in-plane effective fields. The detailed CIMS loops with varying θ_1 were measured without any applied external fields for the $L1_0$ -Fe₄₅Cr₅Pt₅₀ sample, as depicted in Figure 3b. Notably, the most significant field-free phenomenon occurs in the configuration of $\theta_1 = 0^\circ$ or 180° at all instances, and the switching polarity for $\theta_1 = 0^\circ$ is anticlockwise, whereas that for $\theta_1 = 180^\circ$ is clockwise. For the configuration of $\theta_1 = 90^\circ$, the switching loop disappears, indicating that the magnetization switching cannot be driven by current. The angular dependence of in-plane effective field H_{eff} and ΔR_s is depicted in Figure 3c, where H_{eff} can be quantified by the offset of the equivalent magnetic field, and ΔR_s is defined as the variations in Hall resistance after pulsing currents at $+22$ and -22 mA, respectively. Both of them can be fitted using a cosine function with a twofold-symmetric performance. Therefore, the in-plane effective field induced by Cr doping tends to correspond to the FeCrPt [110] direction. To understand this symmetry-dependent field-free switching, the in-plane magnetic anisotropy energy (MAE) in $L1_0$ -FeCrPt was determined based on first-principles calculation, as presented in Figure 3d, which

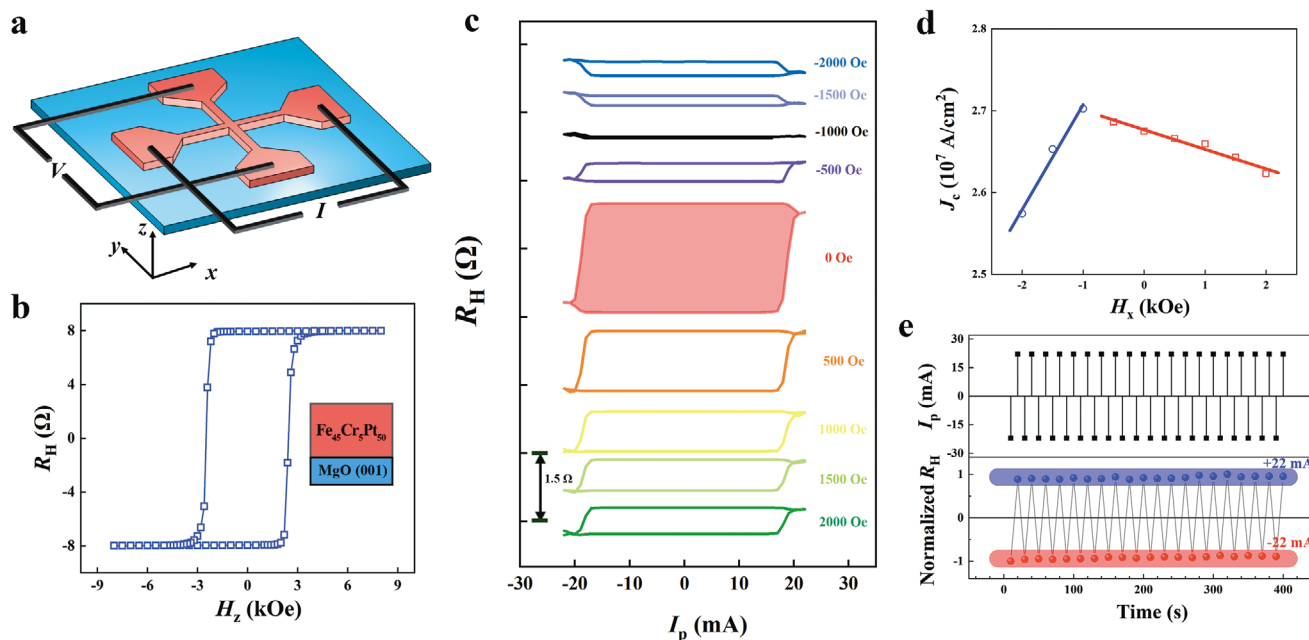


Figure 2. Field-free current-induced magnetization switching. a) Schematic of patterned Hall bar for electrical transport measurements. b) Anomalous Hall loop of $L1_0$ -Fe₄₅Cr₅Pt₅₀ single layer. c) Field dependence of SOT switching of 5-nm-thick $L1_0$ -Fe₄₅Cr₅Pt₅₀ film. d) Critical switching current density (J_c) as a function of H_x . e) Zero field repeatable SOT switching under successive pulsed currents of ± 22 mA with opposite polarities.

suggests a typical twofold symmetry with the easy axis parallel to FeCrPt [110] direction and the hard axis oriented toward^[1–10] direction corresponding to the θ_1 dependence of ΔR_S . Therefore, the introduction of Cr causes a canted magnetization component that favors [110] direction, as depicted in Figure 3e. These results indicated that twofold angular-dependent field-free switching in $L1_0$ -FeCrPt should have an intrinsic origin related to the in-plane magnetocrystalline anisotropy.

Further experiments were conducted with varying Cr content to systematically elucidate the influence of Cr doping on field-free switching induced by SOT. The high-quality epitaxial structure with $L1_0$ -ordered phase was appropriately retained under the involvement of diluted Cr, including the performance with qualified PMA. Nonetheless, excessive doping concentrations can potentially deteriorate the PMA, and Cr doping up to 12.5% results in the absence of PMA in films. Further evidence is detailed in Supporting Information S4. As observed from Figure 4a–c, the current-induced switching loops under zero field and the critical field at which the switching signal disappears for $L1_0$ -Fe_{50–x}Cr_xPt₅₀ with $x = 2.5, 7.5,$ and 10 indicate a similar feasibility of deterministic field-free SOT switching in these three structures. The Cr doping-dependent total in-plane intrinsic effective fields were quantified, as illustrated in Figure 4d (red line), which revealed a nonmonotonic evolution with x ranging from 0 to 10 in Fe_{50–x}Cr_xPt₅₀ films. A significant peak value of ≈ 1000 Oe emerges at $x = 5$. According to recent studies of single-layer films, a bulk DMI induced by the disintegration of inversion symmetry resulting from the asymmetric distribution of the element content was proposed in ferrimagnets GdFeCo,^[44] and a gradient-driven DMI effective field was verified to enable a field-free switching in single-layer films such as CoTb.^[41] Therefore, the DMI effective field induced by the composition gradient can be reasonably responsible for the considerable effective field in the current experiments. Based

on the magnetic droplet nucleation model, the DMI effective field H_{DMI} in $L1_0$ -Fe_{50–x}Cr_xPt₅₀ samples with $x = 0, 2.5, 5, 7.5,$ and 10 was quantified with the method proposed by Kim et al.,^[45] as depicted in Figure 4d (black line), which is much smaller than the experimental values for SOT switching. The detailed information is presented in Supporting Information S5. Accordingly, an additional type of effective field must exist to facilitate the SOT-driven magnetization switching, which is interpreted as the aforementioned exchange coupling field H_{exc} . The exchange coupling field (H_{exc}) as a function of Cr concentration was obtained after subtracting the corresponding values of H_{DMI} , as presented in Figure 4d (blue dashed line), exhibiting a remarkable feature with nonmonotonic variation. Furthermore, the anisotropic field H_K monotonically decreased with the increasing Cr concentrations, as indicated in Figure S6d, (Supporting Information). Therefore, the addition of Cr elements disintegrates the rotational symmetry of the spin torques and reduces the switching energy barrier.

The spin orbit effective field of Fe_{50–x}Cr_xPt₅₀ samples was estimated based on harmonic Hall voltage measurements. In particular, the first (V_{ω}) and second ($V_{2\omega}$) harmonic Hall signals for 5% Cr doped samples under an in-plane magnetic field ranging from -3000 to $+3000$ Oe are depicted in the inset of Figure 4e. The longitudinal effective field H_L can be expressed as

$$H_L = -2 \frac{B_x \pm 2\xi B_y}{1 - 4\xi^2} \quad (1)$$

where, B_x is defined as $\left[\frac{\partial V_{2\omega}}{\partial H} / \frac{\partial^2 V_{\omega}}{\partial H^2} \right]_x$, and ξ denotes the ratio of the planar Hall voltage to the anomalous Hall voltage. The value of ξ for $L1_0$ -FeCrPt with Cr doping contents of 0%, 2.5%, 5%, 7.5%, and 10% was 0.082, 0.061, 0.039, 0.031, and 0.016, respectively. Therefore, it was approximately equal to zero

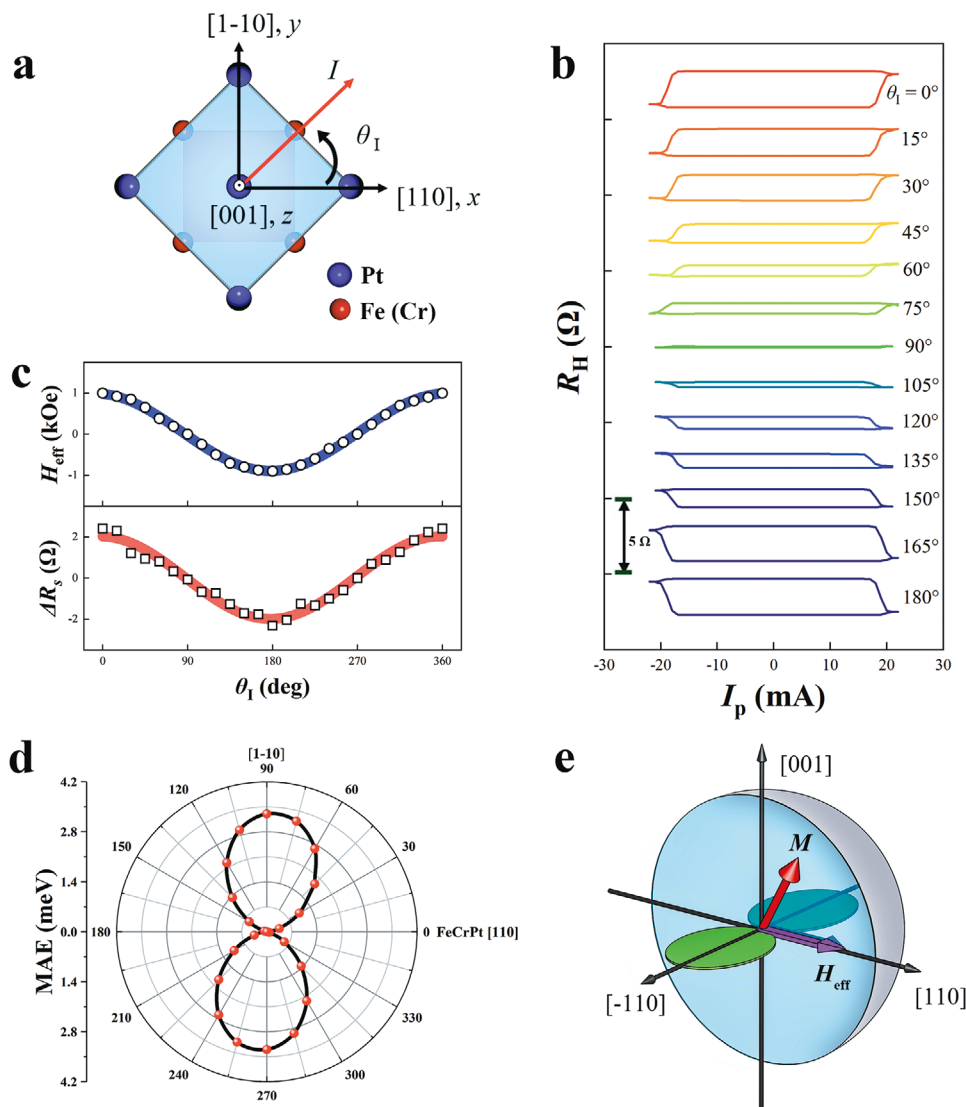


Figure 3. Angle-dependent switching measurement in $L1_0\text{-Fe}_{50-x}\text{Cr}_x\text{Pt}_{50}$ films. a) Definition of current-flowing direction (θ). Current is applied along the hall bar, which bears an azimuth angle of θ with respect to $[110]$ direction. b) Current-induced magnetization switching for hall bars with varying θ . c) Current angle dependence of in-plane effective field and ΔR_s for SOT-induced magnetization switching. Blue/red line denotes a cosine fit to the data. d) Calculated azimuthal angular-dependent magnetic anisotropy energy in xy plane of FeCrPt films. e) Schematic illustration of magnetization configurations and in-plane effective fields in $L1_0\text{-FeCrPt}$.

(refer to Supporting Information S7). The current dependence of H_L is represented in Figure S8b (Supporting Information). According to the linear fitting, we calculated the spin torque efficiency (H_L/J) with various Cr doping contents, which exhibited a diminishing trend with increasing Cr concentrations, as depicted in Figure 4e. On the contrary, the field-free critical switching current density J_{ffc} decreased with the increasing Cr concentrations (Figure 4f; blue points), which is contrary to the inverse correlation to H_L . According to the simplified models in the macrospin limit,^[17,27,46,47] J_c can be expressed as

$$J_c = \frac{e \mu_0 M_s t_{\text{FM}} (H_k - \sqrt{2} |H_x|)}{\hbar \theta_{\text{SH}}} = \frac{J (H_k - \sqrt{2} |H_x|)}{2H_L} \quad (2)$$

Therefore, a switching factor γ for characterizing the hardness of SOT switching in PMA systems can be defined as

$(H_L/J)/H_k$. A monotonic increase in γ with Cr doping explains the requirement of a low J_{ffc} . In addition, the calculated switching efficiency η_{SOT} that represents the ratio of anisotropy field and switching current density was $87 \text{ k Oe per } 10^8 \text{ A cm}^{-2}$ for 5% Cr doping, which is in accordance to the reported study of $L1_0\text{-FePt}$ with a comparable thickness.^[36] These results demonstrated the contribution of Cr doping toward the SOT-driven magnetization switching of the alloy films owing to the significant reduction in energy barrier. Note that the consideration of the thermal effect is essential for accurately estimating the current-induced magnetization switching.^[48] In $L1_0\text{-FeCrPt}$ films, the temperature variations caused by the current-induced Joule heating was negligible (refer to Supporting Information S10). Additionally, Zhao et al.^[49] reported an asymmetric SOT-induced switching between up-to-down and down-to-up magnetized states in Ta/CoFeB/MgO multilayers in case the assisting field

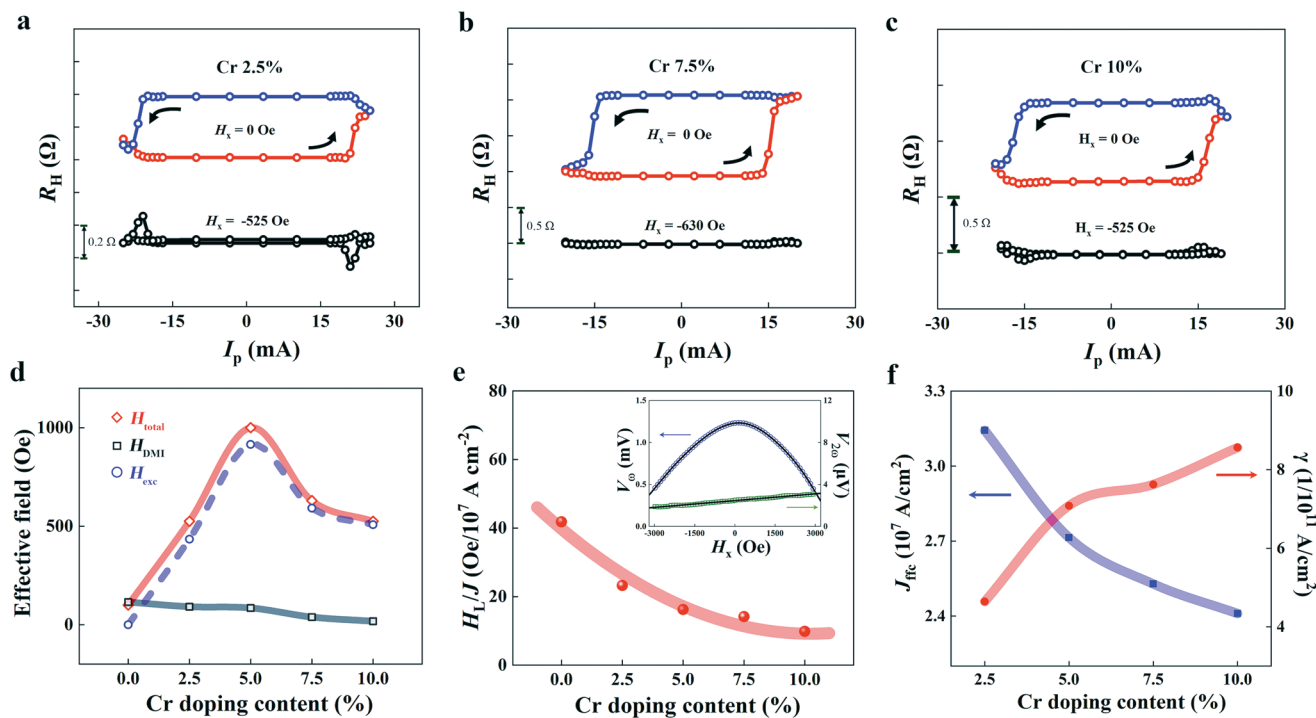


Figure 4. Cr content dependence of field-free SOT switching and in-plane effective field induced by Cr doping. a–c) Field-free SOT switching loops under zero and critical fields corresponding to the disappearance of switching signal for $L1_0$ - $\text{Fe}_{50-x}\text{Cr}_x\text{Pt}_{50}$ with $x = 2.5, 7.5,$ and 10 . d) Total in-plane effective field obtained under current-induced switching experiments (red line), DMI effective field (black line) related to DM interaction, and exchange coupling fields H_{exc} (blue dashed line) after subtracting the corresponding values of DMI field plotted as a function of Cr concentration. e) Longitudinal spin-torque efficiencies for varying Cr contents. Red line acts as a guide to the eye. Inset: first and second harmonic Hall signals as a function of in-plane magnetic field H_x under 3 mA in $\text{Fe}_{45}\text{Cr}_5\text{Pt}_{50}$ film. f) Field-free critical switching current density (J_{fc}) and switching factor γ , defined as $(H_L/J)/H_k$ is a function of Cr contents in $\text{Fe}_{50-x}\text{Cr}_x\text{Pt}_{50}$ films.

direction was not collinear with the electric current, thereby revealing the importance of the transverse SOT effective field on magnetization switching. For the SOT switching of FeCrPt, the assisting field can be replaced by the in-plane effective field and the angular-dependent critical switching current signifies a symmetric SOT switching feature. The detailed discussion is presented in Supporting Information S11.

2.3. Exchange Coupling Effective Field and First-Principles Calculation

To further comprehend the mechanism responsible for the in-plane effective field generated by Cr doping, we discussed the magnetic exchange coupling combined with first-principles calculation. Theoretically, the $L1_0$ structure would be maintained with the substitution of Fe with Cr, producing a striking difference in the magnetic exchange interaction. According to recent reports,^[43] a strong AFM coupling with antiparallel-aligned Fe and doped Cr moments in $L1_0$ -ordered FeCrPt structure was demonstrated using X-ray magnetic circular dichroism techniques. Moreover, a magnetically frustrated system, emerging from the competition of FM Fe–Fe, and AFM Cr–Cr (Fe) exchange interactions, was established after introducing the Cr. This frustration produces a slight tilt of magnetization from the z -axis and accommodates an in-plane H_{exc} term similar to the exchange bias field supplied by the antiferromagnets.

This additional H_{exc} term enables spin torques to disintegrate the rotational symmetry and enables SOT switching without external magnetic fields. Furthermore, a reasonable model corresponding to varying Cr concentrations was addressed to elaborate the nonmonotonic evolution of the in-plane effective field. As the Cr was introduced with a lower concentration ($<5\%$), the presence of more isolated Cr would generate a stronger H_{exc} , thereby generating a robust in-plane H_{exc} , as illustrated in Figure 5a. However, the nearest-neighbor (NN) Cr–Cr pairs started to appear with the increasing Cr concentrations. In this configuration, the NN Fe–Cr spins favored the opposite alignment, but strong AFM Cr–Cr pairs (denoted as J_3) would force the next-nearest-neighbor (NNN) Fe–Cr spins toward parallel alignment (denoted as J_2) against the AFM arrangement, thereby exhibiting a frustrated behavior, as depicted in Figure 5b. The resulting frustration tends to perturb the AFM order between Fe and Cr atoms, resulting in a reduced in-plane H_{exc} .

To account for the total energy without external magnetic fields, the following Hamiltonian was considered.^[43]

$$H = \sum_{(i \neq j)} J_{ij} S_i \cdot S_j - \sum_{(i)} K_u S_i^2 \quad (3)$$

where, S_i denotes the spin at site i . The two energy terms describe the Heisenberg exchange parameters (J_{ij}) and the uniaxial magnetic anisotropy constant (K_u). According to the

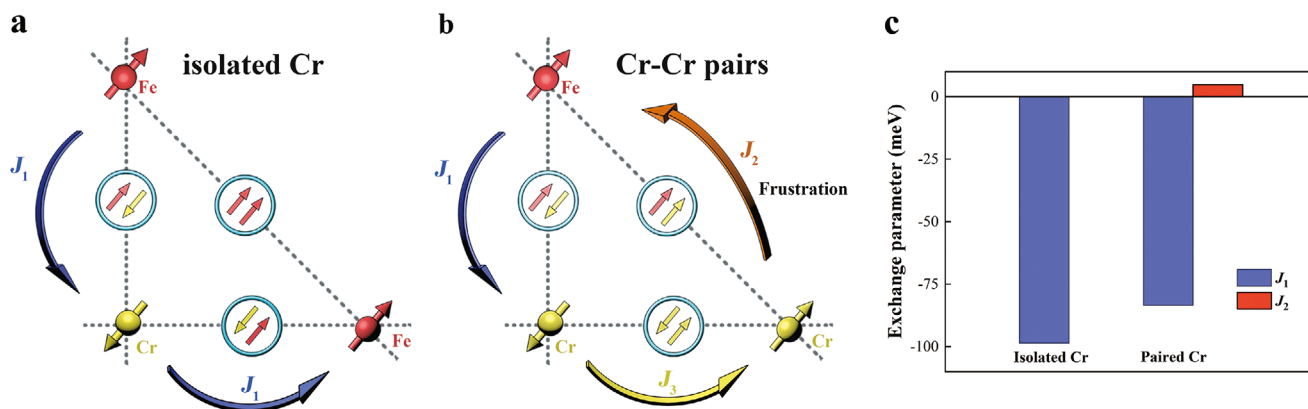


Figure 5. Various Cr configurations induced AFM exchange coupling interaction from first-principles calculation, a) Schematic of exchange interactions with formation of isolated Cr. b) Schematic of exchange interaction with formation of Cr–Cr pairs. c) NN Fe–Cr AFM exchange strength from first-principles calculation based on various types of Cr.

frustrated $J_1 - J_2$ Heisenberg model, the effective Hamiltonian for Fe–Cr interactions can be expressed as

$$H_{\text{Fe,Cr}} = J_1 \sum_{(ij)} \mathbf{S}_i \cdot \mathbf{S}_j - J_2 \sum_{(ij)} \mathbf{S}_i \cdot \mathbf{S}_j \quad (4)$$

where, the parameters J_1 and J_2 denote the NN and NNN exchange interactions, respectively. The sums $\sum_{(i,j)}$ and $\sum_{(i,j)}$ in

Eq. (4) were applied over all the pairs of NN and NNN spins, respectively. Based on the above scenario, first-principles calculation provides a theoretical result corresponding to the model, which verifies the reduced NN AFM exchange interaction between the Fe and Cr atoms owing to the presence of Cr–Cr pairs, as illustrated in Figure 5c. Further detailed information related to the calculations is presented in Supporting Information S12. These results provided theoretical support for the scheme of the aforementioned model, and simultaneously, confirmed the in-plane effective field primarily originating from the AFM exchange interaction between Fe and Cr.

For the bulk-SOT-nature $L1_0$ -FePt structure, spin current can be induced under a spin anomalous Hall effect (SAHE), whose polarization should be parallel to the magnetization axis at all instances.^[50] Generally, the spins accumulated in a single ferromagnetic layer under SAHE cannot exert torques on its own magnetization. However, if FM exhibits strong spin–orbit coupling (SOC) and inversion symmetry disorientation, the transverse spin current generated by this SHE is regarded as magnetization independent and its polarization is perpendicular to the current as well as its flowing direction.^[51–55] Previously, the origin of SOT has been investigated with an interpretation of inversion asymmetry dominated by the stain gradient because of nonuniform vertical composition.^[36,37,56] In general, to perform field-free SOT switching, an efficient strategy involves the introduction of an in-plane effective field such as exchanges bias field,^[17–19] interlayer coupling field,^[20,42] and gradient-driven DMI effective field^[41] to serve as an external magnetic field and disorient the switching symmetry of magnetization. Alternatively, an out-of-plane effective field H_{effz} can be directly produced by manipulating the spin-polarized direction σ of the spin current to deviate from y and generate

a z -polarized component such as interface engineering,^[57] magnetic spin Hall effect,^[58] or selecting the materials with low crystalline symmetry such as WTe_2 ^[59] and $L1_1$ -CuPt^[28] as a spin source. However, the direct generation of the latter H_{effz} was typically dependent on the multilayers with FM(AFM)/NM/FM or NM/FM structure, which cannot be achieved using only a single ferromagnetic layer. In $L1_0$ -FePt configuration, the substitution of Cr for Fe maintains the advantages of the $L1_0$ structure to retain its PMA, and it produces a considerable intrinsic in-plane effective field that can be ascribed to the involvement of the AFM exchange interaction between Fe and Cr for realizing a field-free switching. This method may be extended to alternative single-FM-layered structures to achieve field-free SOT switching, where an external magnetic field is required in advance to obtain the deterministic magnetization switching. Moreover, a smaller current is required to reverse the magnetization without external magnetic fields owing to the reduced switching energy barrier, which is advantageous for practical applications. On the contrary, the in-plane effective field induced by introducing Cr presents a nonmonotonic evolution with increasing Cr contents. This finding is consistent with the model of magnetic exchange interaction corresponding to the exchange strength of Fe and Cr. For Cr doping ranging within 0–5% in $\text{Fe}_{50-x}\text{Cr}_x\text{Pt}_{50}$ films, the in-plane effective field derived from the canted AFM coupling interaction is proportional to the Cr doping concentrations. The corresponding effective field at 5% Cr doping is obtained up to ≈ 1000 Oe, thereby signifying the feasibility of replacing an applied external magnetic field to perform SOT switching, which is essential for novel spintronic devices. However, a further increase in Cr contents will increase the probability of determining the nearest Cr–Cr pairs. Moreover, such spin arrangement produces an intense frustrated behavior owing to the strong NN Cr–Cr AFM coupling and reduces the in-plane effective field induced by Fe–Cr interactions. Although the current-induced switching has been determined in the $L1_0$ -FePt single layer, the physical mechanisms of partial switching are still controversial to date. Thus, more rigorous theoretical calculations and systematic experimental studies are expected to provide more effective information, which is beyond the scope of the current study.

3. Conclusion

In summary, the deterministic two fold angular-dependent field-free magnetization switching was demonstrated in the Cr-doped $L1_0$ -ordered single-layer $Fe_{50-x}Cr_xPt_{50}$, wherein the tailored strength of the exchange coupling interaction was deemed as vital for generating an in-plane effective field. Notably, as the large effective field originated from Cr doping within a single layer, no constraints were involved on the applied magnetic fields to achieve SOT switching, and it simplified the sample structure to provide greater flexibility in the device design. In addition, the considerable tunneling magnetoresistance (TMR) ratio has been already demonstrated in $L1_0$ -FePt-based magnetic tunnel junctions.^[30] Therefore, the Cr-doped $L1_0$ -FePt films presented in this study can be feasibly integrated into SOT memory devices with TMR readout. This study establishes a practical route for utilizing the potential of $L1_0$ -FePt materials in SOT devices, and accordingly, facilitates the applications of SOT in single ferromagnets for energy-efficient and scalable spintronic memory and logic devices.

4. Experimental Section

Sample Growth and Device Fabrication: All epitaxial $Fe_{50-x}Cr_xPt_{50}$ ($x = 0, 2.5, 5, 7.5, 10, \text{ and } 12.5$) films were deposited onto MgO (001) substrates using molecular beam epitaxy (MBE) from individual Fe, Pt, and Cr sources under a base pressure $\leq 7 \times 10^{-11}$ mbar. The MgO substrates were cleaned by acetone and isopropanol in an ultrasound bath and annealed at 750 °C for 2 h after a degas process for 15 min at 850 °C in the MBE chamber prior to the deposition. For deposition of $Fe_{50-x}Cr_xPt_{50}$, the temperature was set at 500 °C, followed by 30 min of in situ annealing at 600 °C to promote the formation of high-quality $L1_0$ phase in the $Fe_{50-x}Cr_xPt_{50}$ alloy. The Cr content x was varied within 0–12.5 at.% by altering the deposition rates at almost constant (Fe+Cr):Pt ratio. In addition, the nominal deposition rate for $Fe_{50-x}Cr_xPt_{50}$ was 0.01 nm s^{-1} , and the deposited films were cooled to room temperature prior to the deposition of 2 nm MgO and 2 nm Cr protection layers. After deposition, the films were patterned into 10 μm Hall bars under UV lithography and argon ion milling.

Structure and Composition Characterization: The formation of the epitaxial structure and high-quality surface was identified by in situ reflection high-energy electron diffraction (RHEED) and X-ray diffraction (XRD) with $Cu\text{-}K\alpha$ radiation. STEM and EDS characterizations were performed using a spherical-aberration-corrected FEI Themis Z microscope.

Transport Properties Measurements: For AHE and DMI measurements, a DC current of 0.5 mA was applied along the FePt or FeCrPt [110] direction defined as x -axis. During current-induced magnetization switching measurements, a pulsed DC electrical current (Keithley 6221) with a duration of 1 ms was applied for each data point. After 10 s, the Hall voltage V_{dc} was recorded by Keithley 2182A using a small DC excitation current (500 μA). The Hall resistance $R_H = V_{dc}/I_{dc}$ was used to characterize the magnetization state. Moreover, a Hall probe was inserted in the probe station to detect the actual magnetic field value during measurements, thereby ensuring the absence of any H_{ext} contributions caused by remanent fields. For harmonics measurements, two SR830 lock-in amplifiers were used to detect the first and second harmonic Hall voltage induced by an AC current of 133.33 Hz. All measurements were conducted at room temperature.

Supporting Information

Supporting Information is available from the Wiley Online Library or from the author.

Acknowledgements

H.L. and Y.Z. contributed equally to this work. This work was supported by the National Key Research and Development Program of China (Grant No. 2019YFB2005800), the Natural Science Foundation of China (Grant Nos. 51625101, 52130103, 12174426, 11874082, 12104486, 11934017, 11921004 and 51971026), the ISF-NSFC Joint Research Program (Grant Nos. 51961145305), the State Key Laboratory for Advanced Metals and Materials (Grant No. 2019Z-10), Beijing Natural Science Foundation Key Program (Grant Nos. Z190007, Z200007), and the Fundamental Research Funds for the Central Universities Grant FRF-TP-16-001C2.

Conflict of Interest

The authors declare no conflict of interest.

Data Availability

The data that support the findings of this study are available from the corresponding authors upon reasonable request.

Keywords

field-free switching, $L1_0$ -FeCrPt, magnetic frustration, spin-orbit torque

Received: January 17, 2022

Revised: April 10, 2022

Published online: April 30, 2022

- [1] I. M. Miron, G. Gaudin, S. Auffret, B. Rodmacq, A. Schuhl, S. Pizzini, J. Vogel, P. Gambardella, *Nat. Mater.* **2010**, *9*, 230.
- [2] I. M. Miron, K. Garello, G. Gaudin, P. J. Zermatten, M. V. Costache, S. Auffret, S. Bandiera, B. Rodmacq, A. Schuhl, P. Gambardella, *Nature* **2011**, *476*, 189.
- [3] L. Q. Liu, O. J. Lee, T. J. Gudmundsen, D. C. Ralph, R. A. Buhrman, *Phys. Rev. Lett.* **2012**, *109*, 096602.
- [4] L. Q. Liu, C. F. Pai, Y. Li, H. W. Tseng, D. C. Ralph, R. A. Buhrman, *Science* **2012**, *336*, 555.
- [5] J. Kim, J. Sinha, M. Hayashi, M. Yamanouchi, S. Fukami, T. Suzuki, S. Mitani, H. Ohno, *Nat. Mater.* **2013**, *12*, 240.
- [6] X. Fan, J. Wu, Y. Chen, M. J. Jerry, H. Zhang, J. Q. Xiao, *Nat. Commun.* **2013**, *4*, 1799.
- [7] N. Sato, F. Xue, R. M. White, C. Bi, S. X. Wang, *Nat. Electron.* **2018**, *1*, 508.
- [8] G. Q. Yu, *Nat. Electron.* **2018**, *1*, 496.
- [9] G. Yang, C. Ciccarelli, J. W. A. Robinson, *APL Mater.* **2021**, *9*, 050703.
- [10] I. M. Miron, T. Moore, H. Szabolcs, L. D. Buda-Prejbeanu, S. Auffret, B. Rodmacq, S. Pizzini, J. Vogel, M. Bonfim, A. Schuhl, G. Gaudin, *Nat. Mater.* **2011**, *10*, 419.
- [11] M. Jamali, K. Narayanapillai, X. Qiu, L. M. Loong, A. Manchon, H. Yang, *Phys. Rev. Lett.* **2013**, *111*, 246602.
- [12] P. Wadley, B. Howells, J. Železný, C. Andrews, V. Hills, R. P. Campion, V. Novák, K. Olejník, F. Maccherozzi, S. S. Dhesi, S. Y. Martin, T. Wagner, J. Wunderlich, F. Freimuth, Y. Mokrousov, J. Kuneš, J. S. Chauhan, M. J. Grzybowski, A. W. Rushforth, K. W. Edmonds, B. L. Gallagher, T. Jungwirth, *Science* **2016**, *351*, 587.
- [13] S. Y. Bodnar, L. Smejkal, I. Turek, T. Jungwirth, O. Gomonay, J. Sinova, A. A. Sapozhnik, H. J. Elmers, M. Klau, M. Jourdan, *Nat. Commun.* **2018**, *9*, 348.

- [14] R. Yoshimi, K. Yasuda, A. Tsukazaki, K. S. Takahashi, M. Kawasaki, Y. Tokura, *Sci. Adv.* **2018**, 4, easat9989.
- [15] A. Chernyshov, M. Overby, X. Y. Liu, J. K. Furdyna, Y. Lyanda-Geller, L. P. Rokhinson, *Nat. Phys.* **2009**, 5, 656.
- [16] M. Jiang, H. Asahara, S. Sato, T. Kanaki, H. Yamasaki, S. Ohya, M. Tanaka, *Nat. Commun.* **2019**, 10, 2590.
- [17] S. Fukami, C. Zhang, S. DuttaGupta, A. Kurenkov, H. Ohno, *Nat. Mater.* **2016**, 15, 535.
- [18] Y. W. Oh, S. H. Chris Baek, Y. M. Kim, H. Y. Lee, K. D. Lee, C. G. Yang, E. S. Park, K. S. Lee, K. W. Kim, G. Go, J. R. Jeong, B. C. Min, H. W. Lee, K. J. Lee, B. G. Park, *Nat. Nanotechnol.* **2016**, 11, 878.
- [19] A. van den Brink, G. Vermeij, A. Solignac, J. Koo, J. T. Kohlhepp, H. J. M. Swagten, B. Koopmans, *Nat. Commun.* **2016**, 7, 10854.
- [20] Y. C. Lau, D. Betto, K. Rode, J. M. Coey, P. Stamenov, *Nat. Nanotechnol.* **2016**, 11, 758.
- [21] Y. Cao, Y. Sheng, K. W. Edmonds, Y. Ji, H. Z. Zheng, K. Y. Wang, *Adv. Mater.* **2020**, 32, 1907929.
- [22] G. Q. Yu, P. Upadhyaya, Y. B. Fan, J. G. Alzate, W. J. Jiang, K. L. Wong, S. Takei, S. A. Bender, L. T. Chang, Y. Jiang, M. Lang, J. S. Tang, Y. Wang, Y. Tserkovnyak, P. K. Amiri, K. L. Wang, *Nat. Nanotechnol.* **2014**, 9, 548.
- [23] C. K. Safer, E. Jue, A. Lopez, L. Buda-Prejbeanu, S. Auffret, S. Pizzini, O. Boulle, I. M. Miron, G. Gaudin, *Nat. Nanotechnol.* **2016**, 11, 143.
- [24] K. M. Cai, M. Y. Yang, H. L. Ju, S. M. Wang, JiY. , B. H. Li, EdmondsK. W. , ShengY. , ZhangB. , ZhangN. , LiuS. , H. Z. Zheng, K. Y. Wang, *Nat. Mater.* **2017**, 16, 712.
- [25] Q. L. Ma, Y. F. Li, D. B. Gopman, Y. P. Kabanov, R. D. Shull, C. L. Chien, *Phys. Rev. Lett.* **2018**, 120, 117703.
- [26] S. Chen, J. Yu, Q. Xie, X. Zhang, W. Lin, L. Liu, J. Zhou, X. Shu, R. Guo, Z. Zhang, J. Chen, *ACS Appl. Mater. Interfaces* **2019**, 11, 30446.
- [27] M. X. Wang, W. L. Cai, D. Q. Zhu, Z. H. Wang, J. Kan, Z. Y. Zhao, K. H. Cao, Z. L. Wang, Y. G. Zhang, T. R. Zhang, C. Park, J.-P. Wang, A. Fert, W. S. Zhao, *Nat. Electron.* **2018**, 1, 582.
- [28] L. Liu, C. Zhou, X. Shu, C. Li, T. Zhao, W. Lin, J. Deng, Q. Xie, S. Chen, J. Zhou, R. Guo, H. Wang, J. Yu, S. Shi, P. Yang, S. Pennycook, A. Manchon, J. Chen, *Nat. Nanotechnol.* **2021**, 16, 277.
- [29] Y. Du, H. Gamou, S. Takahashi, S. Karube, M. Kohda, J. Nitta, *Phys. Rev. Appl.* **2020**, 13, 054014.
- [30] M. Yoshikawa, E. Kitagawa, T. Nagase, T. Daibou, M. Nagamine, K. Nishiyama, T. Kishi, H. Yoda, *IEEE Trans. Magn.* **2008**, 44, 2573.
- [31] A. Kohn, N. Tal, A. Elkayam, A. Kovács, D. Li, S. G. Wang, S. Ghannadzadeh, T. Hesjedal, R. C. C. Ward, *Appl. Phys. Lett.* **2013**, 102, 062403.
- [32] G. Yang, D. L. Li, S. G. Wang, Q. L. Ma, S. H. Liang, H. X. Wei, X. F. Han, T. Hesjedal, R. C. C. Ward, A. Kohn, A. Elkayam, N. Tal, X. G. Zhang, *J. Appl. Phys.* **2015**, 117, 083904.
- [33] T. Seki, K. Utsumiya, Y. Nozaki, H. Imamura, K. Takanashi, *Nat. Commun.* **2013**, 4, 1726.
- [34] W. A. Challener, C. B. Peng, A. V. Itagi, D. Karns, W. Peng, Y. G. Peng, X. M. Yang, X. B. Zhu, N. J. Gokemeijer, Y. T. Hsia, G. Ju, R. E. Rottmayer, M. A. Seigler, E. C. Gage, *Nat. Photon.* **2009**, 3, 220.
- [35] M. Weisheit, S. Fähler, A. Marty, Y. Souche, C. Poinignon, D. Givord, *Science* **2007**, 315, 349.
- [36] M. Tang, K. Shen, S. J. Xu, H. L. Yang, S. Hu, W. M. Lu, C. J. Li, M. S. Li, Z. Yuan, S. J. Pennycook, K. Xia, A. Manchon, S. M. Zhou, X. P. Qiu, *Adv. Mater.* **2020**, 32, 2002607.
- [37] L. Liu, J. H. Yu, R. González-Hernández, C. J. Li, J. Y. Deng, W. N. Lin, C. H. Zhou, T. J. Zhou, J. Zhou, H. Wang, R. Guo, H. Y. Yoong, G. M. Chow, X. F. Han, B. Dupé, J. Železný, J. Sinova, J. S. Chen, *Phys. Rev. B* **2020**, 101, 220402.
- [38] S. Q. Zheng, K. K. Meng, Q. B. Liu, J. K. Chen, J. Miao, X. G. Xu, Y. Jiang, *Appl. Phys. Lett.* **2020**, 117, 242403.
- [39] D. Céspedes-Berrolcal, H. Damas, D. Maccariello, P. Tang, A. Arriola-Córdova, P. Vallobrá, Y. Xu, J.-L. Bello, E. Martin, S. Migot, J. Ghanbaja, S. Zhang, M. Hehn, S. Mangin, C. Panagopoulos, V. Cros, A. Fert, J.-C. Rojas-Sánchez, *Adv. Mater.* **2021**, 33, 2007047.
- [40] R. Q. Zhang, L. Y. Liao, X. Z. Chen, T. Xu, L. Cai, M. H. Guo, H. Bai, L. Sun, F. H. Xue, J. Su, X. Wang, C. H. Wan, H. Bai, Y. X. Song, R. Y. Chen, N. Chen, W. J. Jiang, X. F. Kou, J. W. Cai, H. Q. Wu, F. Pan, C. Song, *Phys. Rev. B* **2020**, 101, 214418.
- [41] Z. Y. Zheng, Y. Zhang, V. Lopez-Dominguez, L. Sánchez-Tejerina, J. C. Shi, X. Q. Feng, L. Chen, Z. L. Wang, Z. Z. Zhang, K. Zhang, B. Hong, Y. Xu, Y. G. Zhang, M. Carpentieri, A. Fert, G. Finocchio, W. S. Zhao, P. K. Amiri, *Nat. Commun.* **2021**, 12, 4555.
- [42] X. Xie, X. Zhao, Y. Dong, X. Qu, K. Zheng, X. Han, X. Han, Y. Fan, L. Bai, Y. Chen, Y. Dai, Y. Tian, S. Yan, *Nat. Commun.* **2021**, 12, 2473.
- [43] N. Y. Schmidt, R. Mondal, A. Donges, J. Hintermayr, C. Luo, H. Ryll, F. Radu, L. Szunyogh, U. Nowak, M. Albrecht, *Phys. Rev. B* **2020**, 102, 214436.
- [44] D. H. Kim, M. Haruta, H. W. Ko, G. Go, H. J. Park, T. Nishimura, D. Y. Kim, T. Okuno, Y. Hirata, Y. Futakawa, H. Yoshikawa, W. Ham, S. Kim, H. Kurata, A. Tsukamoto, Y. Shiota, T. Moriyama, S. B. Choe, K. J. Lee, T. Ono, *Nat. Mater.* **2019**, 18, 685.
- [45] S. Kim, P.-H. Jang, D.-H. Kim, M. Ishibashi, T. Taniguchi, T. Moriyama, K.-J. Kim, K.-J. Lee, T. Ono, *Phys. Rev. B* **2017**, 95, 220402.
- [46] L. J. Zhu, D. C. Ralph, R. A. Buhrman, *Phys. Rev. Appl.* **2021**, 15, 024059.
- [47] K.-S. Lee, S.-W. Lee, B.-C. Min, K.-J. Lee, *Appl. Phys. Lett.* **2013**, 102, 112410.
- [48] L. Liu, T. Zhao, L. Ren, C. Zhou, W. Lin, X. Shu, J. Zhou, Q. Xie, J. Chen, *ACS Appl. Electron. Mater.* **2021**, 3, 2483.
- [49] W. Fan, J. Zhao, M. Tang, H. Chen, H. Yang, W. Lü, Z. Shi, X. Qiu, *Phys. Rev. Appl.* **2019**, 11, 034018.
- [50] T. Seki, S. Iihama, T. Taniguchi, K. Takanashi, *Phys. Rev. B* **2019**, 100, 144427.
- [51] W. L. Yang, J. W. Wei, C. H. Wan, Y. W. Xing, Z. R. Yan, X. Wang, C. Fang, C. Y. Guo, G. Q. Yu, X. F. Han, *Phys. Rev. B* **2020**, 101, 064412.
- [52] H. Wu, S. A. Razavi, Q. Shao, X. Li, K. L. Wong, Y. Liu, G. Yin, K. L. Wang, *Phys. Rev. B* **2019**, 99, 184403.
- [53] W. Wang, T. Wang, V. P. Amin, Y. Wang, A. Radhakrishnan, A. Davidson, S. R. Allen, T. J. Silva, H. Ohldag, D. Balzar, B. L. Zink, P. M. Haney, J. Q. Xiao, D. G. Cahill, V. O. Lorenz, X. Fan, *Nat. Nanotechnol.* **2019**, 14, 819.
- [54] J. Cramer, A. Ross, S. Jaiswal, L. Baldrati, R. Lebrun, M. Kläui, *Phys. Rev. B* **2019**, 99, 104414.
- [55] D. Tian, Y. Li, D. Qu, S. Y. Huang, X. Jin, C. L. Chien, *Phys. Rev. B* **2016**, 94, 020403.
- [56] L. J. Zhu, D. C. Ralph, R. A. Buhrman, *Adv. Funct. Mater.* **2021**, 31, 2103898.
- [57] S. C. Baek, V. P. Amin, Y. W. Oh, G. Go, S. J. Lee, G. H. Lee, K. J. Kim, M. D. Stiles, B. G. Park, K. J. Lee, *Nat. Mater.* **2018**, 17, 509.
- [58] S. Hu, D.-F. Shao, H. Yang, M. Tang, Y. Yang, W. Fan, S. Zhou, E. Y. Tsymlal, X. Qiu, *ArXiv* **2021**, 2, 2103.09011.
- [59] D. MacNeill, G. M. Stiehl, M. H. D. Guimarães, R. A. Buhrman, J. Park, D. C. Ralph, *Nat. Phys.* **2016**, 13, 300.